Suppressing filamentation instability due to laser beam self-filtering

Dmitry Silin, Efim Khazanov

A.V. Gaponov-Grekhov Institute of Applied Physics of the Russian Academy of Sciences, Nizhny Novgorod, Russia

Abstract: The development of small-scale self-focusing in a nonlinear Kerr medium after preliminary self-filtering of a laser beam propagating in free space is studied numerically. It is shown that, under definite conditions, due to self-filtering, filamentation instability (beam splitting into filaments) either occurs at significantly larger values of the B-integral, or does not occur at all. In the latter case, there develops a honeycomb instability revealed in this work. This instability is the formation of a random honeycomb structure in the beam cross section. It is shown that self-filtering can significantly increase the permissible values of the B-integral, at which the beam quality remains acceptable.

Key words: small-scale self-focusing, self-filtering, filamentation instability, honeycomb instability

1. INTRODUCTION

The small-scale self-focusing (SSSF) is, actually, filamentation instability of a plane wave propagating in a medium with cubic nonlinearity. The SSSF manifests itself as a fast amplification of wave components with high spatial frequencies, which ultimately leads to beam

10.1017/hpl.2024.9

splitting into filaments, thus deteriorating the beam quality and significantly increasing the risk of optical elements breakdown. SSSF was first theoretically predicted by V. Bespalov and V. Talanov [1], experimentally confirmed in [2-6], and the theory was further developed in the works [7-12]. At the linear stage of development the SSSF is reduced to the energy transfer from a plane wave to spatial noise, i.e. to amplification of seed noise waves. The gain K depends on the angle $\theta=k_\perp/k$ between the wave vectors of the noise component $k_\perp$ and plane wave $k=n_0k_0$ (n_0 is the linear index of refraction). In the linear theory, K has a maximum value at the angle

$$\theta_{max} = \sqrt{\frac{2n_2 I}{n_0}}, \tag{1}$$

where I is the intensity of a plane wave and the refractive index of a nonlinear medium is defined as $n=n_0+n_2I$ (n_2 is the nonlinear index of refraction). In the linear approximation, the maximum gain is

$$K(\theta_{max}) = \cosh(2B), \tag{2}$$

where B is the B-integral:

$$B = k_0 n_2 I l, \tag{3}$$

and l is the length of the nonlinear medium.

In the classical SSSF works, nanosecond pulses were considered, where the beam was usually split into filaments at $B>3$. The SSSF studies for femtosecond pulses [13-16] showed that there is a significant difference between nano- and femtosecond pulses, which allows using beam self-filtering as a method for SSSF suppression. There are two mechanisms of beam self-filtering during propagation in free space. In the first of them (we will call it spatial self-filtering) the noise components propagate at an angle to the main beam and, if the beam passed a rather large length of the free space, these components go outside the beam aperture. According to the second mechanism called temporal self-filtering, the noise components lag behind the main beam, which, in the case of short pulses, allows reducing noise at the input to the nonlinear medium and, hence, suppressing the SSSF. The efficiency of both self-filtering methods depends on the angle θ_{max}. For nanosecond pulses, a typical θ_{max} value is about 1 mrad, which impedes self-filtering as it demands a too large propagation length. At the same time, for femtosecond pulses,

https://doi.org/10.1017/hpl.2024.9 Published online by Cambridge University Press

the intensity is as a rule 3 orders of magnitude higher and, according to (1), the typical values of θ_{max} are tens of mrad, which makes self-filtering an efficient mechanism of noise reduction for θ of the order of θ_{max}.

The linear theory of SSSF gives a correct result only at an early stage of instability development, when the power of the amplified noise is low. From a practical point of view, this stage is not so interesting, since because of small noise the beam retains an acceptable quality. Of major interest is the determination of the B-integral values at which hot spots leading to optical breakdown appear in the beam, or at which a significant part (e.g., 10%) of the plane wave energy is converted into noise. Thus, to quantify the efficiency of self-filtering for suppressing SSSF, the nonlinear regime should be considered. It is also worth mentioning that the experimental results demonstrated a significant suppression of SSSF, which cannot be explained by the existing theoretical concepts [17]. One of the goals of our paper is to propose such a concept.

This work is devoted to a detailed numerical simulation of the nonlinear stage of the SSSF taking into account various self-filtering parameters of the input pulse. The conditions under which self-filtering leads to significant suppression of the filamentation instability are found, and a new type of instability is discovered.

2. PROBLEM STATEMENT

The propagation of the field in a medium with Kerr nonlinearity will be studied using the nonlinear Schrödinger equation (NSE) [18] of the form:

$$\frac{\partial A}{\partial z} + \frac{i}{2k}\Delta_{\perp}A + i\frac{3\pi\omega_0\chi^{(3)}}{2n(\omega_0)c}|A|^2A = 0, \tag{4}$$

where A is the complex amplitude of the field, z is the longitudinal component, c is the speed of light in vacuum, $\omega_0 = ck_0$, $\Delta_{\perp}$ is the transverse Laplace operator, and $\chi^{(3)}$ is the cubic nonlinear susceptibility. To simplify the computations, we omitted in the NSE the time dependence of the complex field amplitude and neglected the finite transverse size of the beam. The simulation was made for a square 5x5 mm beam region with periodic boundary conditions.

At the entrance to the nonlinear medium (z=0), the field is represented as a plane wave with superimposed noise. The noise is determined by the manufacturing quality of the optical

https://doi.org/10.1017/hpl.2024.9 Published online by Cambridge University Press

elements through which the beam has passed, and is usually characterized by a one-dimensional power spectral density PSD(k_x). The PSD(k_x) function typical of the optical elements is well approximated by the power dependence [19-21]:

$$\mathrm{PSD}(k_x) = \frac{\Phi_1}{k_x^{\beta}}, \tag{5}$$

where Φ_1 and β are constants. The constant β takes on various values from 1 to 2 in different works and spatial frequency ranges, β=1.55 is the most frequent one. As shown in the work [22], the PSD (5) corresponds to the two-dimensional power spectral density of the noise PSD2($k_\perp$) in the form

$$\mathrm{PSD2}(k_\perp) = \frac{\Phi_2}{k_\perp^{\beta+1}}, \tag{6}$$

where Φ_2 is constant. Thus, for PSD2($k_\perp$) we adopt the dependence (6), where β=1.55.

The beam self-filtering is modeled using the expression for temporal self-filtering [23] at which the free space for a Gaussian pulse in time domain is the filter of spatial frequencies (angles θ) with transmittance

$$T_{time}(\theta) = \exp\left\{-\left(\ln(2)\frac{L}{\lambda}\frac{\theta^2}{N}\right)^2\right\} = \exp\left\{-\frac{\theta^4}{\theta_{thr}^4}\right\}, \tag{7}$$

where L is the distance passed by the pulse in free space, $\lambda=2\pi/k_0$, N is the ratio of the pulse duration to the period of the field, and θ_{thr} is the threshold value of the angle of self-filtering (the angle at which $T_{time}(\theta)=1/e$). Further, for definiteness, we will assume θ_{thr}=4 mrad, which corresponds, e.g., to L=1.6 m for the pulse duration 60 fs and wavelength 910 nm.

The expression (7) was obtained for an ideal Gaussian pulse. In practice, the contrast of femtosecond pulses is limited, as a pedestal outside the main pulse restricts the filter contrast (7), which was taken into consideration in numerical simulations. It is worth noting that at spatial filtering the free space is a filter with transmittance $T_{space}(\theta)$, the shape of which [16] is close to (7), but the contrast may be much higher, as there is almost no spatial pedestal. An important feature of both $T_{time}(\theta)$ and $T_{space}(\theta)$ is a very sharp decrease when θ exceeds the threshold value θ_{thr}.

https://doi.org/10.1017/hpl.2024.9 Published online by Cambridge University Press

When a laser pulse propagates through optical elements, inaccuracy in manufacturing the shape of optical surfaces gives rise to phase noise (imaginary part of the complex field amplitude), and various scratches and dust particles to amplitude noise (real part of the complex field amplitude). During the propagation in free space, the phase and amplitude noise transform into each other; therefore, after passing through a large number of optical elements, it can be assumed with a high degree of certainty that the noise is half phase and half amplitude. It is this noise that was used in the simulation of the SSSF. In this work, we will neglect the noise arising from the refraction at the input surface of a nonlinear medium.

An example of intensity and phase distribution in the beam at the input of the nonlinear element is given in Fig. 1. The noise in Fig. 1 has been filtered according to (7) with self-filtering threshold θ_{thr}=4 mrad. The input noise power P_{noise} is about 0.02% of the power P_0 of the principal wave. This noise gives the ratio of the maximum intensity in the beam I_{max} to the mean intensity I_0 of about 1.07.

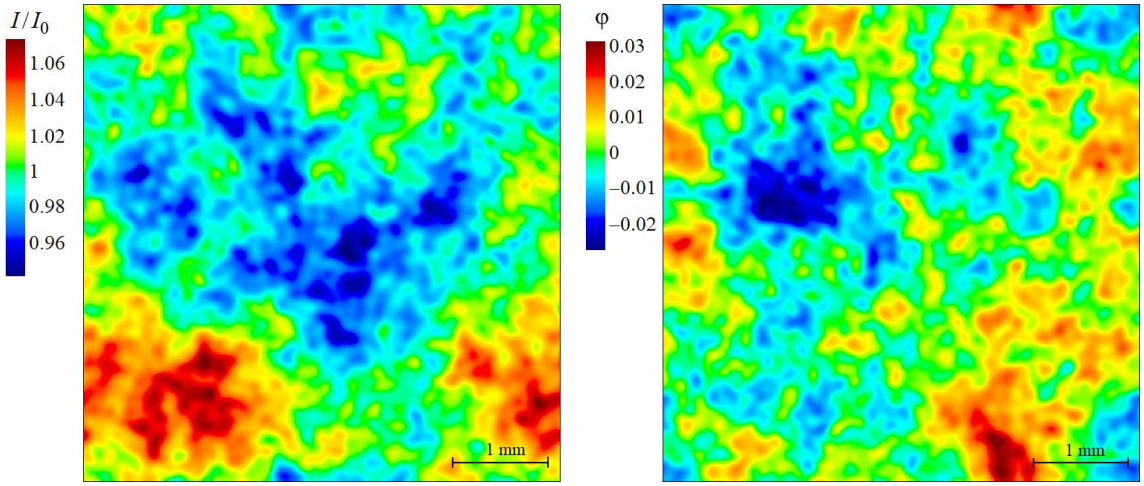

Fig. 1. Intensity and phase distribution in the input beam within 5x5 mm area.

The main goal of the simulation was to see the difference in the development of instability in two cases: $\theta_{max}<\theta_{\text{thr}}$=4 mrad and $\theta_{max}>\theta_{thr}$. The first case is typical for nanosecond and picosecond pulses, for which θ_{max} is about 1 mrad; therefore, self-filtering does not affect the noise components with maximal increment. The case with $\theta_{max}>\theta_{thr}$ is typical for femtosecond pulses, for which θ_{max} is usually tens of mrad and the noise components with maximal increment are filtered at the input to the nonlinear medium, and only components with a much lower gain remain. Hence, we performed numerical simulations for four θ_{max}: 1 mrad, 3 mrad, 10 mrad, and

https://doi.org/10.1017/hpl.2024.9 Published online by Cambridge University Press

30 mrad. If fused silica is used as the nonlinear medium, then the above values of θ_{max} correspond to the intensity I_0 = 3 GW/cm^2, 27 GW/cm^2, 300 GW/cm^2, and 2.7 TW/cm^2, respectively. The calculations were performed up to the values of the B-integrals, at which a significant power of the principal wave was converted into noise. With a further increase in the B-integral, the sizes of bright spots become smaller than the cell size of the computational grid, which varied from 2.5 to 20 μm in different calculations.

3. RESULTS OF NUMERICAL SIMULATION

The calculated noise spectra $S(\theta)$=PSD2($k_\perp$=k·θ) are shown in Figs. 2a and 3a for the original beam (B=0) and the beam that has passed in a nonlinear medium distances corresponding to B=3, 4, 5, 6; the self-filtering contrast is 10^8. Figure 2a is for θ_{max}=1 mrad and Fig. 3a is for θ_{max}=3 mrad. The dashed curves correspond to the gain $K(\theta)$ in the linear (without plane wave depletion) regime [18]:

$$K = 1 + \frac{2}{\frac{2\theta^2}{\theta_{max}^2} - \frac{\theta^4}{\theta_{max}^4}} \cdot sinh^2\left\{B\sqrt{\frac{2\theta^2}{\theta_{max}^2} - \frac{\theta^4}{\theta_{max}^4}}\right\} \quad (8)$$

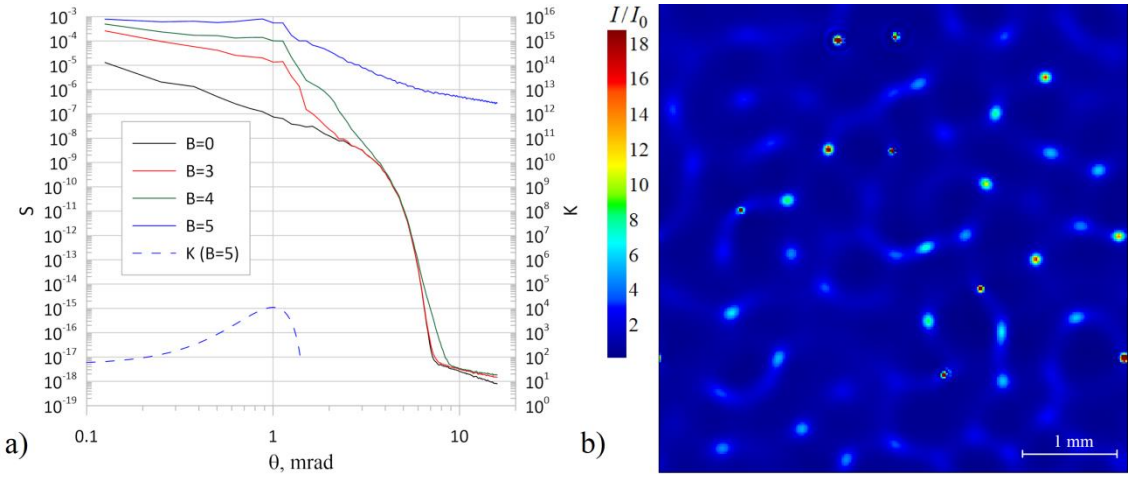

Fig. 2. SSSF for θ_{max}=1 mrad at noise filter contrast 10^8: a) noise spectrum (solid curves), gain $K(\theta)$ in the linear regime for B=5 (dashed curve); b) intensity distribution in the beam for B=5 within 5x5 mm area.

For B=3, 4 maximum gain is seen at θ=θ_{max}, which is quite expected. For B=5, 6 the radiation collapses, the noise spectrum approaches white noise, with the noise power increasing by many orders of magnitude, even outside the instability region, i.e. at θ>$\sqrt{2}\theta_{max}$. The intensity

https://doi.org/10.1017/hpl.2024.9 Published online by Cambridge University Press

distribution in the beam is illustrated in Fig. 2b (for θ_{max}=1 mrad, B=5) and in Fig. 3b (for θ_{max}=3 mrad, B=6). The collapse is seen in Figs. 2b and 3b. The radiation is focused into a large amount of filaments of huge intensity: I_{max}/I_0=274 for θ_{max}=1 mrad and I_{max}/I_0=187 for θ_{max}=3 mrad. In this case p=0.28 and 0.45, where $p=P_{\text{noise}}/P_0$, i.e. 28% and 45% of the beam power have been converted into noise, respectively. The power in each filament is $P_{fil} \approx 2.25P_{cr}$, where

$$P_{cr} = \frac{0.174\lambda^2}{n_2 n_0} \tag{9}$$

is the critical power of self-focusing [24], and a typical distance between the filaments is $\lambda/(n_0 \cdot \theta_{max})$. Thus, for $\theta_{max}<\theta_{thr}$ we have obtained a classical filamentation instability. The maximum values of I/I_0 on the color palettes in Figs. 2b and 3b are determined by excluding 0.05% of points with maximum intensity. Therefore, the maximum values of I/I_0 on the palettes are less than of I_{max}/I_0.

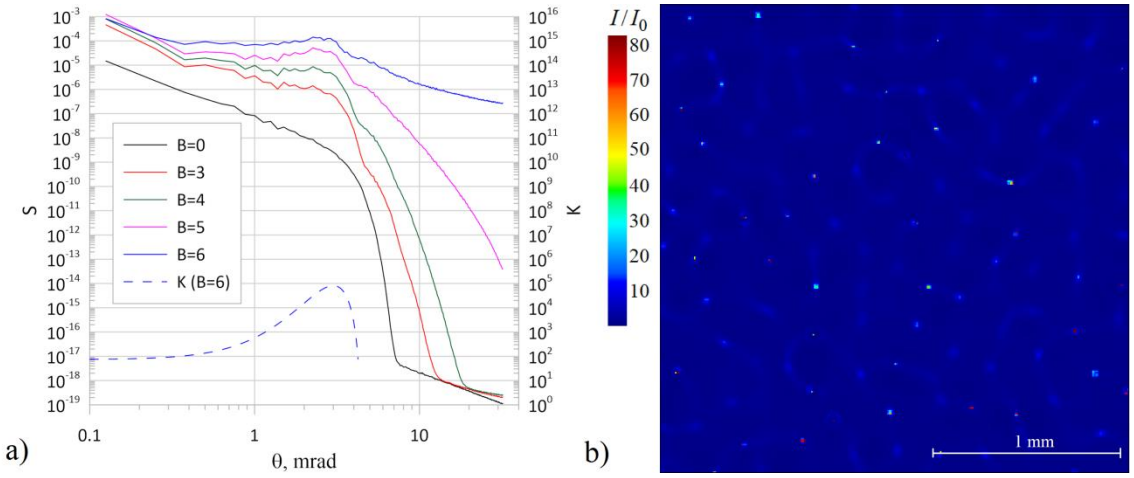

Fig. 3. SSSF for θ_{max}=3 mrad at noise filter contrast 10^8: a) noise spectrum (solid curves), $K(\theta)$ in the linear regime for B=6 (dashed curve); b) intensity distribution in the beam for B=6 within 2.5x2.5 mm area.

The effect of beam self-filtering is expected to manifest itself at $\theta_{max}>\theta_{thr}$. The noise spectra $S(\theta)$ for θ_{max}=10 mrad are shown in Figs. 4a and 5a for various values of the B-integral. Figure 4a corresponds to the case with self-filtering of the beam before it enters the nonlinear medium with a contrast of 10^8, and Fig. 5a corresponds to the case without self-filtering. In the latter case, the noise gain maximum is at $\theta=\theta_{max}$. There is no such gain maximum in the noise spectra after self-filtering, and the nonlinear stage looks qualitatively different, as is clearly

https://doi.org/10.1017/hpl.2024.9 Published online by Cambridge University Press

demonstrated in Fig. 4b for B=11 (p=0.32). It can be seen that, instead of a large number of bright dots, a random honeycomb structure has appeared. A typical cell size of this structure corresponds to $\lambda/(n_0 \cdot \theta_{thr})$. To the best of our knowledge, such an instability has never been observed before either in numerical simulation or in experiment. We will refer to it as honeycomb instability. The honeycomb structure is preserved with an increase in the B-integral, the intensity in the walls of the honeycombs increases, and their thickness decreases until it becomes less than the cell size of the computational grid. For comparison, the intensity distribution without self-filtering is shown in Fig. 5b for B=6, i.e. for a value significantly smaller than in Fig. 4b. Here, 41% of the beam power was converted into noise (p=0.41), and a classical collapse of the radiation into a large number of bright points with a typical transverse scale $\lambda/(n_0 \cdot \theta_{max})$ is visible. There are two videos of SSSF for θ_{max}=10 mrad (the time scale corresponds to the beam propagation in a nonlinear medium and, accordingly, to the growth of the B-integral) in the supplementary materials for this paper. In one of the videos (Silin_supplementmovie1.avi), the calculation was performed taking into account beam self-filtering, which leads to the development of honeycomb instability. In the second video (Silin_supplementmovie2.avi), there is no beam self-filtering, and filamentation instability develops.

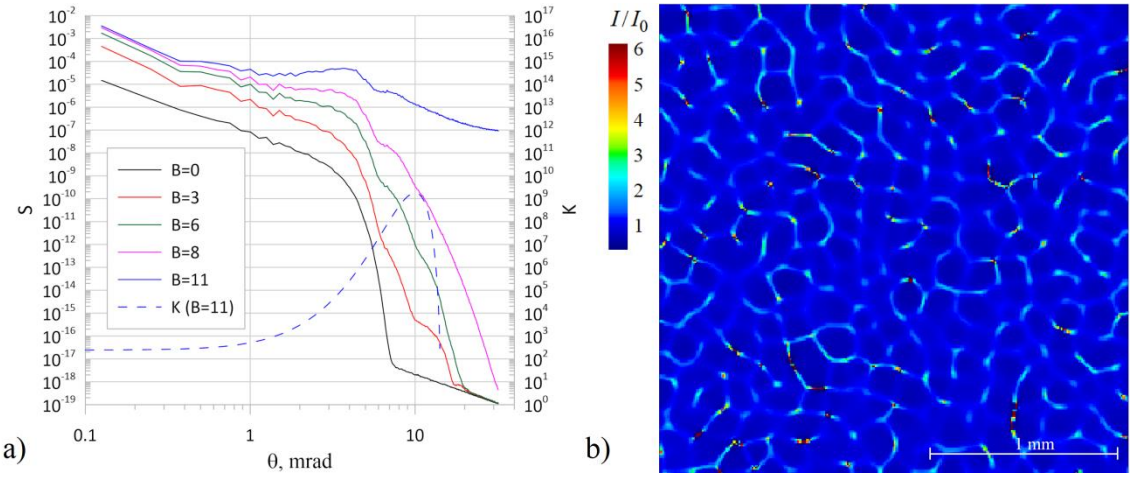

Fig. 4. SSSF for θ_{max}=10 mrad at noise filter contrast 10^8: a) noise spectrum (solid curves), $K(\theta)$ in the linear regime for B=11 (dashed curve); b) intensity distribution in the beam for B=11 within 2.5x2.5 mm area (see Silin_supplementmovie1.avi for $0 \le B \le 11$ within 5x5 mm area).

https://doi.org/10.1017/hpl.2024.9 Published online by Cambridge University Press

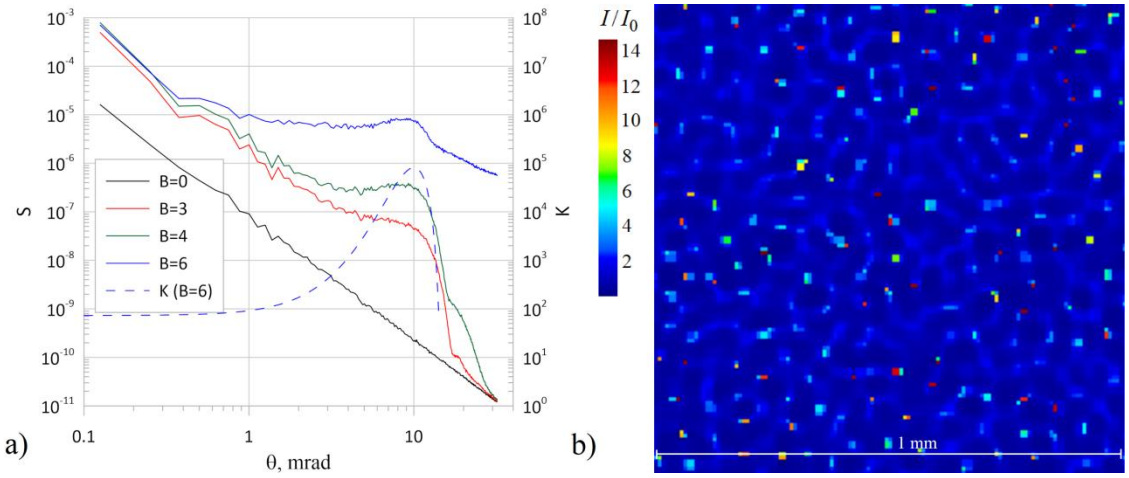

Fig. 5. SSSF for θ_{max}=10 mrad, no self-filtering: a) noise spectrum (solid curves), $K(\theta)$ in the linear regime for B=6 (dashed curve); b) intensity distribution in the beam for B=6 within 1x1 mm area (see Silin_supplementmovie2.avi for $0 \le B \le 6$ within 5x5 mm area).

Now consider the case of θ_{max}=30 mrad that is typical of femtosecond pulses. The noise spectra $S(\theta)$ for different values of the B-integral are shown in Fig. 6a. Despite the beam self-filtering one can see gain maxima at $\theta=\theta_{max}$. We attribute this to the fact that θ_{max}=30 mrad is far from the filtering threshold θ_{thr}=4 mrad, therefore, the amplification of the noise components at $\theta<4$ mrad is very low at the linear stage of the SSSF, and the noise components in the $\theta \sim \theta_{max}$ region are in an advantageous situation despite the self-filtering. This is what differs the case with θ_{max}=30 mrad from the case with θ_{max}=10 mrad, where the components with $\theta<\theta_{thr}$ are advantageous, so the honeycomb instability develops faster than the filamentation one. The intensity distribution in the beam for B=16 is shown in Fig. 6b. It can be seen that the beam collapsed into a large number of random points and there is no honeycomb structure (here p=0.51). For the honeycomb structure to appear in the beam cross section, the development of filamentation instability should be slowed down even more. The numerical simulations have shown that this can be achieved by increasing the noise filter contrast by up to 20 orders of magnitude or more. Naturally, such a level of noise suppression cannot be achieved in practice, even with spatial self-filtering. However, to demonstrate the physical aspect of the problem, we have performed the corresponding numerical simulations.

https://doi.org/10.1017/hpl.2024.9 Published online by Cambridge University Press

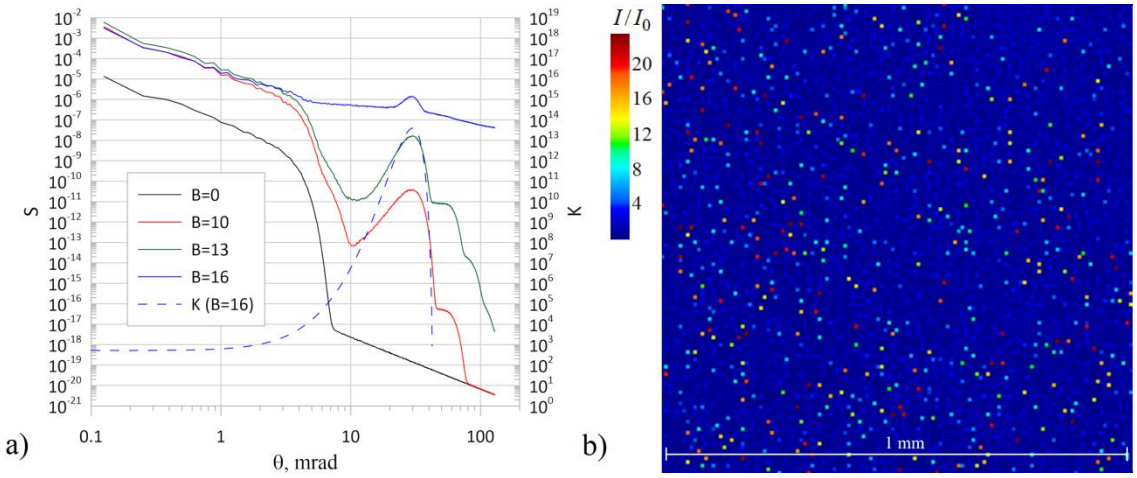

Fig. 6. SSSF for θ_{max}=30 mrad at noise filter contrast 10^8: a) noise spectrum (solid curves), $K(\theta)$ in the linear regime for B=16 (dashed curve); b) intensity distribution in the beam for B=16 within 1x1 mm area.

The noise spectra for θ_{max}=30 mrad at a noise filter contrast of the 24-th order are plotted in Fig. 7a, and the corresponding intensity distribution in the beam for B=27 is presented in Fig. 7b (here p=0.59). In this case, the filamentation instability is inferior to the honeycomb instability. A honeycomb structure with characteristic size $\lambda/(n_0 \cdot \theta_{thr})$ is well seen in the beam.

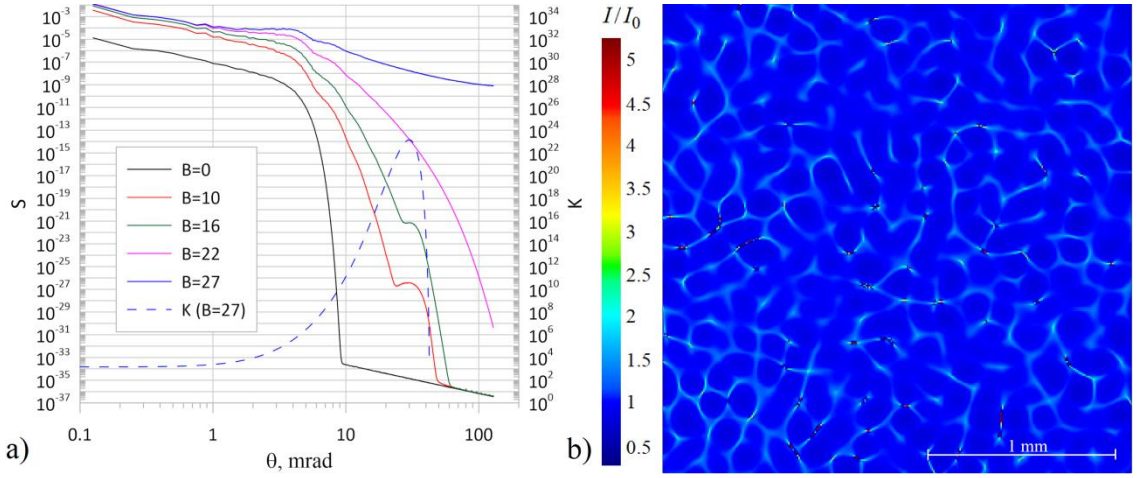

Fig. 7. SSSF for θ_{max}=30 mrad at noise filter contrast 10^{24}: a) noise spectrum (solid curves), $K(\theta)$ in the linear regime for B=27 (dashed curve); b) intensity distribution in the beam for B=27 within 2.5x2.5 mm area.

At the end of this section, we will consider a benchmark to provide some verification of our numerical simulation. Let us calculate the noise gain $K(\theta)$ in the linear mode (there is no depletion of the principal wave). In this case, the gain must coincide with the analytical formula (8). Let θ_{max}=10 mrad and the filter contrast be 10^8, we observed the appearance of a honeycomb

https://doi.org/10.1017/hpl.2024.9 Published online by Cambridge University Press

structure with these parameters (see Fig. 4). However, the input noise level we used produces a discrepancy between the gain $K(\theta)$ obtained from the numerical simulation and formula (8) even at B=1. Therefore, we have reduced the input noise level by two orders of amplitude. In this case, numerical simulation also leads to the appearance of a honeycomb structure; however, at small values of B, the gain coincides with formula (8) with good accuracy. This can be seen in Fig. 8, which shows the noise gain for two values of the B-integral: B=5 and B=8, obtained from numerical simulation and formula (8).

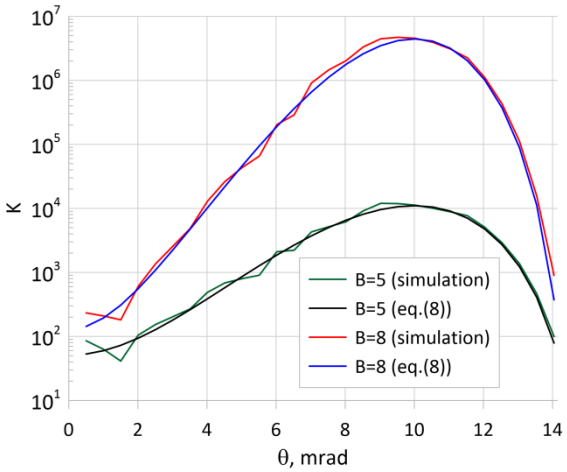

Fig. 8. Comparison of noise gain $K(\theta)$ in linear mode obtained using numerical simulation and formula (8).

4. THE INFLUENCE OF BEAM SELF-FILTERING ON PERMISSIBLE VALUES OF THE B-INTEGRAL

Beam self-filtering allows suppressing the noise components possessing maximum gain at the SSSF, thus increasing the value of the B-integral, at which the beam is not fit for most applications, i.e. an appreciable part of the energy goes into noise, and/or I_{max} becomes significantly larger than I_0. To understand how beam self-filtering affects the permissible values of the B-integral, we will construct various beam parameters as a function of B.

https://doi.org/10.1017/hpl.2024.9 Published online by Cambridge University Press

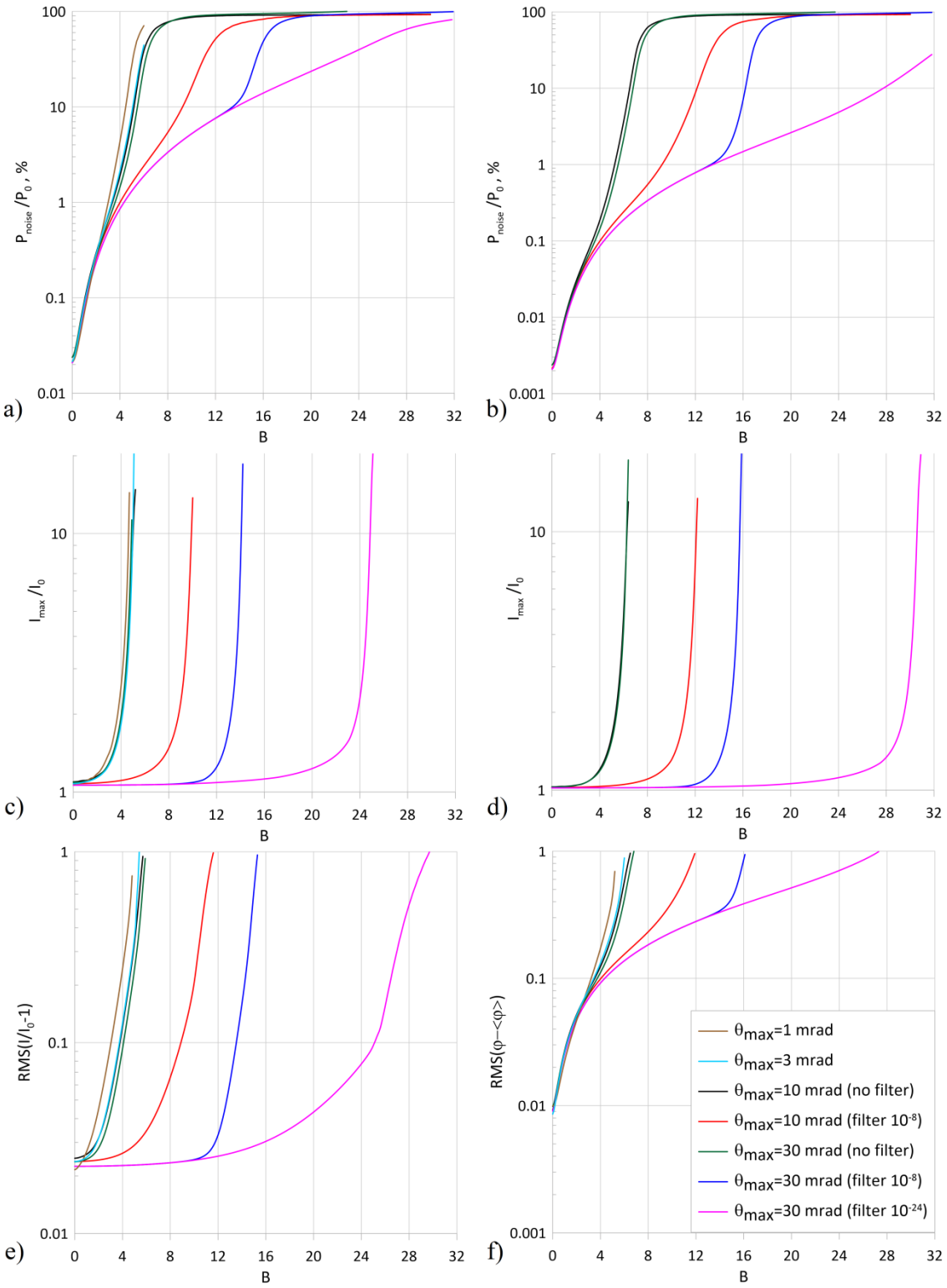

Fig. 9. a), b) Fraction of radiation power converted into noise, c), d) maximum intensity in the beam normalized to mean intensity in the beam, e) RMS intensity in the beam, and f) RMS phase in the beam as a function of B-integral. Curves a), c), e), f) correspond to the level of input noise of about 0.02% of the beam power, curves b), d) are for the level of input noise of about 0.002% of the beam power. Self-filtering threshold θ_{thr}=4 mrad.

https://doi.org/10.1017/hpl.2024.9 Published online by Cambridge University Press

The share of radiation power converted into noise $p=P_{noise}/P_0$ versus B-integral is shown in Fig. 9a,b. The maximum intensity in the beam normalized to mean intensity I_{max}/I_0 versus B-integral is plotted in Fig. 9c,d. The RMS intensity in the beam where the intensity is normalized to the mean intensity $RMS_I=RMS(I/I_0-1)$ as a function of the B-integral is shown in Fig. 9e. Finally, the RMS phase in the beam relative to the mean phase in the beam $RMS_\varphi=RMS(\varphi-\langle\varphi\rangle)$ as a function of the B-integral is plotted in Fig. 9f. Figures 9 a,c,e,f show the curves for the input noise level of 0.02% (this noise level was used for obtaining the results described in Section 3), and Figs. 9 b,d correspond to the input noise level of 0.002%. The curves in Fig. 9 correspond to four values θ_{max}=1 mrad, 3 mrad, 10 mrad, and 30 mrad. The curves for θ_{max}=1 mrad, 3 mrad are plotted for the case of self-filtering. However, since $\theta_{max}<\theta_{thr}$=4 mrad, the self-filtering does not affect the result, so the curves in the absence of self-filtering are the same. For θ_{max}=10 mrad, the curves are plotted both for self-filtering and without it at a contrast of 10^8. For θ_{max}=30 mrad, the curves are plotted for two values of noise filter contrast 10^8 and 10^{24}, as well as without self-filtering. The effect of collapse is clearly demonstrated in Fig. 9c,d – at a definite value of the B-integral, I_{max} increases "almost vertically", despite the logarithmic scale.

From the plots presented in Fig. 9, we can draw the following conclusions. Without noise filtering, an increase in θ_{max} leads to an insignificant decrease in the parameters p, RMS_I, and RMS_φ, while I_{max} remains almost unchanged. Thus, from the point of view of the I_{max} growth, the admissible B-integral does not depend on θ_{max}. Beam self-filtering at small values of the B-integral (B<4) practically does not affect p and RMS_φ, while from the point of view of I_{max} and RMS_I, self-filtering suppresses the SSSF. This means that the amplified noise is phase noise.

With self-filtering, all curves in Figs. 9a-d are notably shifted to the right, which points to a significant increase in the permissible B-integral. The increase in the noise filter contrast increases the admissible B-integral still more. Another important fact is that the decrease in the input noise level affects the increase in the permissible B-integral in different ways. Without self-filtering, as well as for θ_{max}=30 mrad and filter contrast 10^8, when a honeycomb structure is not formed, a decrease in the input noise by a factor of 10 increases the admissible B-integral by ~1.5. At the same time, during self-filtering, when a honeycomb structure appears, the admissible B-integral with the same decrease in the input noise increases by about 2-3 for θ_{max}=10 mrad and filter contrast 10^8 and by about 6-14 for θ_{max}=30 mrad and filter contrast 10^{24}. The permissible values of the B-integral at θ_{max}=30 mrad are given in Table 1 for different values of filter contrast

https://doi.org/10.1017/hpl.2024.9 Published online by Cambridge University Press

and input noise level under the specified criteria I_{max}/I_0<1.5, p<10%. It can be seen from the table that without filtering, the criterion I_{max}/I_0<1.5 is more stringent than p<10%. However, with an increase in contrast, the allowable values of the B-integral in terms of the criterion I_{max}/I_0<1.5 grow faster and, with a high filter contrast, the energy transfer from the principal beam to noise comes to the fore. Note that even with a contrast of 10^6 only, the admissible values of the B-integral become two-digit.

Table 1. Permissible values of the B-integral for θ_{max}=30 mrad

Input noise	Criterion	No filter	6-th order filter	8-th order filter	12-th order filter	24-th order filter
p=0.02%	I_{max}/I_0<1.5	3.5	10.5	12.7	17.1	22.8
	p<10%	5.5	12	13.5	13.8	13.8
p=0.002%	I_{max}/I_0<1.5	5	12.1	14.5	20.4	28.8
	p<10%	6.8	13.9	16.2	20.8	27.8

5. DISCUSSION OF THE RESULTS

The obtained results may be physically interpreted as follows. Without self-filtering, the instability is developing primarily at the spatial frequencies $k_{\perp max}= k_0 n_0 \theta_{max}$ and on the spatial scales $w_{max} = 2\pi/k_{\perp max} = \lambda/(n_0\theta_{max})$ corresponding to the highest increment. From the known expression for the length of self-focusing (the length on which a beam having diameter w and power P_1 collapses) [24]

$$L_{sf} = \frac{0.0925 k_0 n_0 w^2}{\sqrt{\left(\sqrt{P_1/P_{cr}} - 0.852\right)^2 - 0.03}} \qquad (10)$$

it follows that for w=w_{max} the beam collapses at $B \approx 2.3$. The real values are somewhat higher, because for the instability to form inhomogeneities of sufficient amplitude on a plane wave the beam must pass a definite distance. However, self-filtering of high spatial frequencies may result in the concentration of maximum noise power at the spatial frequencies $k_0 n_0 \theta_{thr}$ and on the spatial scales $w_{thr} = \lambda/(n_0\theta_{thr})$, since these scales, although they have a smaller increment, are not subject to filtering. Thus, during self-filtering, there is a competition between the scales w_{max} and w_{thr}. If the contrast is high, and θ_{thr} is a little less than θ_{max} (i.e. the difference in increments is not so

https://doi.org/10.1017/hpl.2024.9 Published online by Cambridge University Press

significant), then the maximum noise power will be concentrated on the w_{thr} scales. Alternatively, if the contrast is low and θ_{thr} is much less than θ_{max}, the scale w_{max} will be a winner. In this case, the SSSF has a classical filamentation character and self-filtering leads to an increase in the admissible value of the B-integral, as the input noise power on the w_{max} scale is significantly reduced. If the scale w_{thr} "wins", then the picture changes qualitatively. The filamentation instability is completely suppressed and the honeycomb instability develops, which is radiation focusing into a line (interface between the cells) rather than into a point, i.e. one-dimensional self-focusing occurs instead of a two-dimensional one. Since the problem is isotropic, the directions of these lines are random, which gives a honeycomb-like spatial pattern (Figs. 4b and 7b) with a typical size w_{thr}. Note that the cell size w_{thr} depends neither on I nor on n_2; therefore, the power per a single cell Iw_{thr} does not depend on n_2.

Let us try to explain the absence of two-dimensional self-focusing. Shortly before the development of filamentation or honeycomb instability (B is 2-3 radians less than in the case of collapse), the intensity distribution in the beam looks similar in both cases. An example of such a distribution is demonstrated in Fig. 10. For the sake of generality, the color scale is not shown in Fig. 10, as it may be different, but I_{max} here exceeds I_0 by several tens of percent. The characteristic scale w (characteristic transverse sizes of the spots) correspond to the scale w_{thr} if $\theta_{max} > \theta_{thr}$ (at a sufficient level of self-filtering contrast) and w_{max} if $\theta_{max} < \theta_{thr}$, or there is no self-filtering. Here, the conditions used to obtain the expression (10) are not fully realized, since there are no isolated round spots for which the self-focusing length could be calculated. One can see in Fig. 10 compact bright (red) spots, but they are located on the elongated spots with a lower intensity. Therefore, the nonlinear phase gradient on the bright spots varies in different directions, resulting in different self-focusing rates in different directions. Further SSSF development depends only on the ratio of the scales w and w_{max} (in other words, on the $\theta_{max}\backslash\theta_{thr}$ ratio). If there is no self-filtering (or $\theta_{max} < \theta_{thr}$), then on the $w=w_{max}$ scale the two-dimensional self-focusing increment significantly exceeds the one-dimensional self-focusing increment, as a result of which the elongated spots break up into separate round ones and classical 2D self-focusing occurs with the formation of filaments. At a high enough level of contrast, self-filtering ($\theta_{max} > \theta_{thr}$) results in the characteristic scale $w=w_{thr} > w_{max}$ on which two-dimensional self-focusing does not have such an advantage over the one-dimensional self-focusing. So, due to a larger nonlinear phase gradient in the transverse direction of the elongated spots than along them,

https://doi.org/10.1017/hpl.2024.9 Published online by Cambridge University Press

one-dimensional self-focusing is faster than the two-dimensional one. As a result, the elongated spots turn into honeycomb borders.

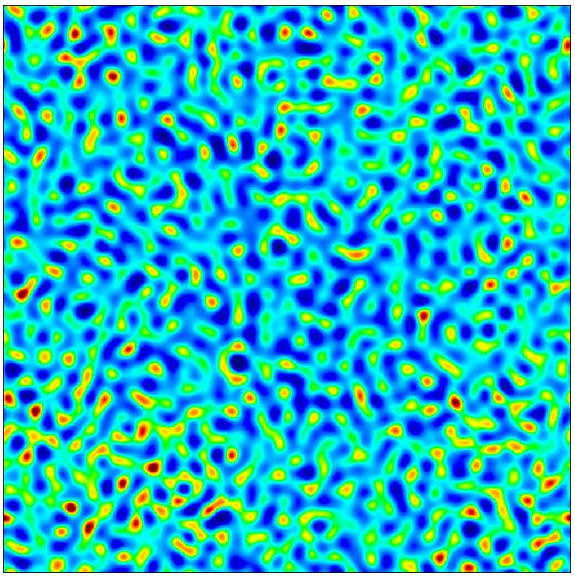

Fig. 10. Example of intensity distribution in a beam shortly before the development of either filamentation or honeycomb instability.

The honeycomb patterns in nonlinear optics were reported in 2002 [25]. There are fundamental differences in the honeycomb structure presented in [25] and in our paper. First, somewhat different equations are solved. We consider the propagation in a medium with cubic nonlinearity (corresponding to the term in the nonlinear Schrödinger equation $\sim|A|^2A$), while in [25] the propagation in a medium with saturation of the linear part of susceptibility is considered (the corresponding term in the equation $\sim A/(1+|A/A_{sat}|^2)$). Second, and most important, is that in our work there occurs one-dimensional small-scale self-focusing into the honeycomb borders, so the intensity of the honeycomb borders becomes significantly higher than the intensity of the honeycomb interiors (see Figs. 4b and 7b), while in [25], on the contrary, the honeycomb borders are darker than the honeycomb interior.

It should be noted that honeycomb instability occurs over a wide range of initial parameters. The above figures present the results when the degree of PSD decay in formula (5) is $\beta=1.55$, and the spatial frequency filter has the form (7). However, numerical simulation has shown that the honeycomb structure in the beam appears for the β values at least in the $0\leq\beta\leq3$ range, and the sharpness of the spatial frequency filter can vary in the range at least from

https://doi.org/10.1017/hpl.2024.9 Published online by Cambridge University Press

$\exp(-\theta^2/\theta_{thr}^2)$ to a step function. A necessary condition for honeycomb instability is sufficient filter contrast, it differs for different parameters. The parameters considered in the article (β=1.55, filter (7) at θ_{thr}=4 mrad, input noise power about 0.02% of the power of the main wave) require a filter contrast of at least 10^6 for θ_{max}=10 mrad, while for θ_{max}=30 mrad a filter contrast of at least 10^{20} is required. In any case honeycomb instability exists (or does not exist) irrespective of random realization of spatial noise used as a boundary condition for eq. (4).

We have considered a stationary instability model, taking into account pulse duration only in the filter transmittance (7). Obviously, allowance for nonstationarity in the NSE (1) will lead to pulse spreading in the course of propagation and, consequently, to a decrease in the effective B-integral, see, for example [17]. This means that the values of admissible B-integral listed in Table 1 will be even higher for fs pulses. A detailed investigation of this issue will be the subject of another publication.

6. CONCLUSION

The results of the performed numerical simulation lead to the following conclusions on the efficiency of beam self-filtering in terms of instability suppression:

1. At $\theta_{max}>\theta_{thr}$, the classical filamentation instability leading to the appearance of bright points in the beam develops slower, i.e. at larger values of the B-integral.

2. With a high self-filtering contrast, the filamentation instability does not develop at all, since it is inferior to the earlier unknown honeycomb instability resulting in a honeycomb structure in which all energy is accumulated within the boundaries between the cells.

3. Beam self-filtering at $\theta_{max}>\theta_{thr}$ significantly increases the admissible values of the B-integral, at which the beam retains acceptable quality: the maximum intensity exceeds the average one by no more than 50% and the fraction of power in the noise does not exceed 10%. The higher the filtering contrast, the larger the admissible values of the B-integral. In the absence of self-filtering, the mentioned intensity increase occurs earlier than 10% of the beam power converts into noise, whereas in the case of self-filtering with a sufficiently high contrast, the opposite is true.

4. The reduction of the fraction of noise power in the input beam with self-filtering increases the admissible B-integral by a much larger value than in the absence of self-filtering.

https://doi.org/10.1017/hpl.2024.9 Published online by Cambridge University Press

5. The study may be a route to explain experimental results [17], which cannot be explained by the existing theoretical concepts.

Funding

Ministry of Science and Higher Education of the Russian Federation (075-15-2020-906, Center of Excellence “Center of Photonics”).

References

1. V. I. Bespalov and V. I. Talanov, “Filamentary structure of light beams in nonlinear liquids,” JETP Lett. **3**(12), 307-310 (1966).
2. Yu S. Chilingarian, “Self-focusing of inhomogeneous laser beams and its effect on stimulated scattering,” JETP **28**(5), 832-835 (1969).
3. E.S. Bliss, D.R. Speck, J.F. Holzrichter, J.H. Erkkila, and A.J. Glass, “Propagation of a high-intensity laser pulse with small-scale intensity modulation,” Appl. Phys Lett. **25**, 448 (1974).
4. A. J. Campillo, S. L. Shapiro, and B. R. Suydam, “Periodic breakup of optical beams due to self-focusing, ” Appl. Phys. Lett. **23**, 628 (1973).
5. A. J. Campillo, S. L. Shapiro, and B. R. Suydam, “Relationship of self-focusing to spatial instability modes,” Appl. Phys. Lett. **24**, 178 (1974).
6. Satish C. Abbi and Herbert Mahr, “Optical filament formation in nitrobenzene resulting from laser intensity inhomogeneities,” Appl. Phys. Lett. **19**, 415 (1971).
7. S. C. Abbi and Nitin C. Kothari, “Growth of Gaussian instabilities in Gaussian laser beams,” J. Appl. Phys. **51**, 1385 (1980).
8. J. Fleck, J. Morris, and E. Bliss, “Small-scale self-focusing effects in a high power glass laser amplifier,” IEEE J. Quantum Electron. **14**, 353-363 (1978).
9. B.R. Suydam, “Effect of refractive-index nonlinearity on the optical quality of high-power laser beams,” IEEE J. Quantum Electron. **11**, 225-230 (1975).
10. S. N. Vlasov and V. E. Yashin, “Suppression of self-focusing in neodymium-glass laser systems using repeaters,” Sov. J. Quantum Electronics **11**, 313-318 (1981).
11. N.N Rosanov and V.A. Smirnov, “Small-scale self-focusing of laser radiation in amplifier systems,” Sov. J. Quantum Electron. **10**, 232 (1980).
12. J.H. Marburger, “Self-focusing: Theory,” Prog. Quantum Electron. **4**, 35-110 (1975).

https://doi.org/10.1017/hpl.2024.9 Published online by Cambridge University Press

13. S.Y. Mironov, V.V. Lozhkarev, V.N. Ginzburg, I.V. Yakovlev, G. Luchinin, A.A. Shaykin, E.A. Khazanov, A.A. Babin, E. Novikov, S. Fadeev, A.M. Sergeev, and G.A. Mourou, “Second-harmonic generation of super powerful femtosecond pulses under strong influence of cubic nonlinearity”, IEEE J. Sel. Top. Quantum Electron. **18**, 7-13 (2012).
14. S. Mironov, V. Lozhkarev, G. Luchinin, A. Shaykin, and E. Khazanov, "Suppression of small-scale self-focusing of high-intensity femtosecond radiation," Applied Physics B: Lasers and Optics **113**, 147-151 (2013).
15. V. N. Ginzburg, A. A. Kochetkov, A. K. Potemkin, and E. A. Khazanov, "Suppression of small-scale self-focusing of high-power laser beams due to their self-filtration during propagation in free space," Quantum Electron. **48**, 325–331 (2018).
16. A. Kochetkov, M, Martyanov, V. Ginzburg, and E. Khazanov, “Self-filtering of beam fluence fluctuations at free space propagation,” Laser Phys. Lett. **20**, 065001 (2023).
17. M. Martyanov, V. Ginzburg, A. Balakin, S. Skobelev, D. Silin, A. Kochetkov, I. Yakovlev, A. Kuzmin, S. Mironov, I. Shaikin, S. Stukachev, A. Shaykin, E. Khazanov, and A. Litvak, "Suppressing small-scale self-focusing of high-power femtosecond pulses," High Power Laser Science and Engineering **11**, e28 (2023).
18. E.A. Khazanov, S.Y. Mironov, and G.A. Mourou, “Nonlinear compression of high-power laser pulses: compression after compressor approach,” Physics-Uspekhi **62**, 1096 (2019).
19. M. L. Spaeth, K. R. Manes, C. C. Widmayer, W. H. Williams, P. K. Whitman, M. A. Henesian, I. F. Stowers, and J. Honig, "National ignition facility wavefront requirements and optical architecture," Optical Engineering **43**, 2854-2865 (2004).
20. E. L. Church, "Fractal surface finish," Applied Optics **27**, 1518-1526 (1988).
21. S. Liu, C. Jin, Y. Zhou, Y. Bai, Y. Zhao, K. Yi, and J. Shao, "Investigation on measurement of mid-frequency wavefront error for large optics in high-power laser system," in Optical Measurement Systems for Industrial Inspection IX, 952536 (2015).
22. V.N. Ginzburg, A.A. Kochetkov, S.Y. Mironov, A.K. Potemkin, D.E. Silin, and E.A. Khazanov, “Features of the Development of the Small-Scale Self-Focusing in Superpower Femtosecond Lasers,” Radiophys. Quantum Electron. **62**, 849-860 (2020).
23. E.A. Khazanov, “Post-compression of femtosecond laser pulses using self-phase modulation: from kilowatts to petawatts in 40 years,” Quantum Electron. **52**, 208 (2022).

https://doi.org/10.1017/hpl.2024.9 Published online by Cambridge University Press

24. V.N. Gol’dberg, V.I. Talanov, and R.E. Erm, "Self-focusing of axially symmetric electromagnetic beams," Radiophys. Quantum Electron. **10**, 368-375 (1967).
25. R. S. Bennink, V. Wong, A. M. Marino, D. L. Aronstein, R. W. Boyd, C. R. Stroud, Jr., and S. Lukishova, "Honeycomb Pattern Formation by Laser-Beam Filamentation in Atomic Sodium Vapor," Phys. Rev. Lett. **88**, 113901 (2002).

https://doi.org/10.1017/hpl.2024.9 Published online by Cambridge University Press